


# Twist-angle-induced boundary-obstructed topological insulator on elastic kagome metamaterials

Zi-Dong Zhang<sup>1</sup>,<sup>1</sup> Ming-Hui Lu,<sup>1,2,\*</sup> and Yan-Feng Chen<sup>1,2</sup>

<sup>1</sup>*National Laboratory of Solid State Microstructures & Department of Materials Science and Engineering, Nanjing University, Nanjing 210093, China*

<sup>2</sup>*Jiangsu Key Laboratory of Artificial Functional Materials, Nanjing University, Nanjing 210093, China*

 (Received 6 July 2023; revised 11 October 2023; accepted 16 October 2023; published 1 November 2023)

Twisted kagome lattices have unusual physical effects upon regulating the twist angle, an additional degree of freedom, which has drawn attention to these lattices. Here, we extend twisted kagome lattices to continuous elastomers and study the dynamics of flexural waves. We confirm that the twist angle can introduce boundary-obstructed topological insulators into topological trivial elastic kagome metamaterials by topological quantum chemistry theory. The kagome metamaterials have degenerate boundary states and twist-angle-dependent corner states. According to corner states corresponding to the inner angles of the modes, the corner states can be divided into two categories, obtuse-corner states and acute-corner states. The operating frequencies of the corner state corresponding to different inner angles are nondegenerate. The twist angle leads to rich and diverse regulations of the corner state. These results reveal hidden topological properties in trivial lattices and add an additional degree of freedom, the twisted angle, to tune higher-order topological insulators.

DOI: [10.1103/PhysRevApplied.20.054002](https://doi.org/10.1103/PhysRevApplied.20.054002)

## I. INTRODUCTION

The extension of quantized electric polarization from dipole moments to multipole moments led to the discovery of higher-order topological insulators (HOTIs), which greatly expanded the class of topological matter [1–5] and has already been realized in photonic systems [6–8], acoustic systems [9–13], and electric circuits [14–16]. The bulk-boundary correspondence in HOTIs can enable functionalities, and thus, has attracted extensive attention, such as zero-dimensional corner states that can realize high- $Q$  resonators [17,18], lasers [19], and switches [20] in two-dimensional second-order topological insulator. In 2017, Bradlyn *et al.* developed the theory of topological quantum chemistry (TQC) to systematically study the topological properties of materials [21]. Recently, this approach was also confirmed as a reliable route to capture higher-order topologies in bosonic systems [22–27]. The HOTI can be diagnosed by checking whether the system is an obstructed atomic insulator (OAI), where the obstructed Wannier charge centers are located at the atom-unoccupied Wyckoff positions (WPs) [28–30]. This method is not only suitable for determining HOTIs in topologically nontrivial phases but also provides a method for finding hidden topological properties in topologically trivial phases, which can

be realized in electronic materials [31–33]. However, so far, it has not been reported in bosonic systems [1,2,6–16].

Maxwell lattices, mechanical frameworks with an average coordination number equal to twice their spatial dimension, are a research hotspot for recent developments in the field of topological mechanics [34–39]. The kagome lattice is a typical Maxwell lattice, where various topological effects, such as the quantum valley Hall effect, quantum spin Hall effect, and high-order topological effects, have been realized [38,39]. Recently, the introduction of an additional degree of freedom, namely, the twist angle, has further enriched the study of kagome lattices [40–48]. Twisted kagome lattices exhibit a special type of duality, whereby a hidden symmetry guarantees that two different configurations (or twist angles) can exhibit identical phonon spectra [40]. An elastic twisted kagome lattice at a critical twist angle exhibits peculiar finite-frequency topological modes [41], corner modes with zero energy [42], and the existence of fragile topological properties [43,44]. So far, the investigation of the topological behavior of two-dimensional twisted kagome lattices has been mainly limited to their intrinsic in-plane mechanics without exploring their out-of-plane response [34–48].

Here, we extend the kagome lattices to continuous elastomers, study the dynamics of flexural waves, and discover hidden topological properties in topologically trivial phases through TQC. We confirm theoretically and experimentally that the twist angle can introduce

\*luminghui@nju.edu.cn

boundary-obstructed topological insulators into elastic kagome metamaterials. The boundary-obstructed elastic topological kagome metamaterials have degenerate boundary states and twist-angle-dependent corner states. We reveal that such corner states are derived from charge accumulation at the boundary of a single obstructed-atomic-limit (OAL) band. The corner states and edge states were confirmed by testing the experimental samples with a laser vibrometer. According to corner states corresponding to the inner angles of the modes, the corner states can be divided into two categories: obtuse-corner states and acute-corner states. The operating frequencies of the corner state corresponding to different inner angles are nondegenerate. The twist angle leads to rich and diverse regulations of the corner state, where the twist angle can adjust its operating

frequency and the frequency difference between the two types of corner states, and it can also make corner states submerge in edge states or bulk states.

## II. DESIGNING TWISTED KAGOME METAMATERIALS IN THE ELASTIC CONTINUUM

Kagome lattices have the characteristic of a continuously adjustable twist angle. The adjustable range of the twist angle is from  $0^\circ$  to  $60^\circ$  because the lattice symmetry does not change with different twist angles, as shown in Fig. 1(a). The initial kagome lattice ( $\theta = 0$ ) has a planar space group,  $P6mm$  (No. 183). The twist kagome lattice ( $\theta \neq 0$ ) is under the  $G = p31m$  space group (No. 157) [40].

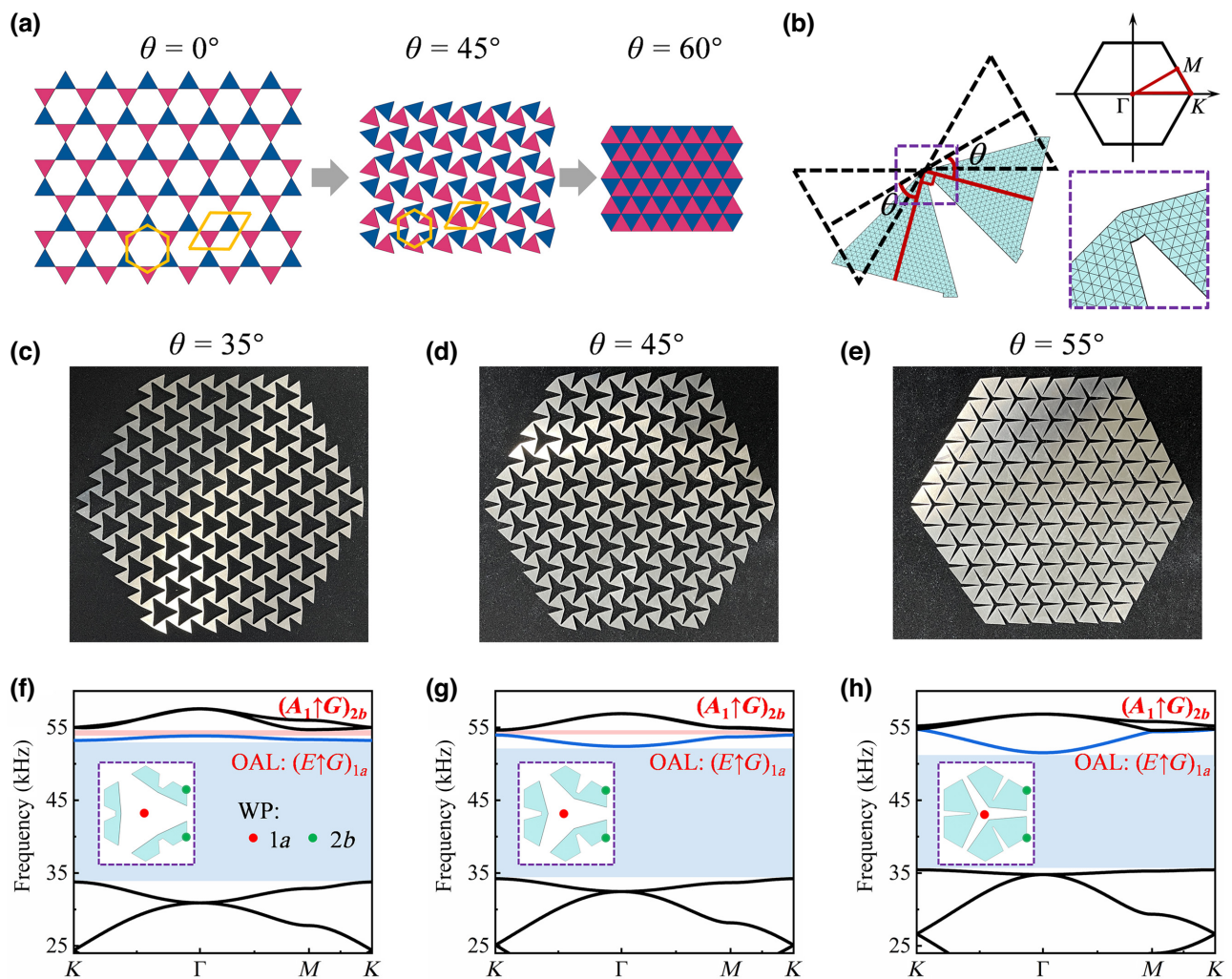


FIG. 1. (a) Schematic diagram of the continuously adjustable twist angle of the twisted kagome lattice. (b) Schematic diagram of the unit cell of the twisted kagome metamaterial, where  $\theta$  is the twist angle, and the corresponding Brillouin zone and an enlarged view of the hinge region. (c)–(e) Photographs of elastic twisted kagome metamaterials with twist angles of  $35^\circ$ ,  $45^\circ$ , and  $55^\circ$ , respectively. (f)–(h) Corresponding band diagram of kagome metamaterials with twist angles of  $35^\circ$ ,  $45^\circ$ , and  $55^\circ$ , respectively. Inset, Wigner-Seitz unit cell of twisted kagome metamaterials labeled with red and green dot markers representing  $1a$  and  $2b$  Wyckoff positions, respectively.

Figure 1(b) shows the transition from a structural lattice configuration to continuous elastomers, in which the triangles are elastic domains and ideal hinges are replaced by ligaments of radius  $r$ . Next, we choose three kinds of twist-angle samples of  $35^\circ$ ,  $45^\circ$ , and  $55^\circ$  as research objects. The corresponding samples were obtained by laser cutting a 2-mm-thick aluminum plate; photographs are shown in Figs. 1(c)–1(e). Here, to extend the research paradigm of the Maxwell lattice, we choose to study the dynamic behavior of out-of-plane displacement instead of in-plane displacement. The resulting band structure of the flexural wave is shown in Figs. 1(f)–1(h) for elastic kagome metamaterials with different twist angles of  $35^\circ$ ,  $45^\circ$ , and  $55^\circ$ , respectively.

Let us take the bands of self-dual kagome metamaterials as an example. There are three isolated bands in the band structures, which are divided into band 7, degenerate band 8, and band 9. The kagome lattices have vanishing bulk polarization; hence, the Wannier centers cannot be determined by bulk polarization [41]. Through the theory of TQC [21], these bands are determined as OAL bands. From finite-element calculations of the high-symmetry-point vibration modes, we determine their irreducible representations, as shown in Fig. 7 (Appendix A). For a set of bands spanned by symmetric exponentially localized Wannier functions, the band representations of these bands can be labeled by the site-symmetry group at Wyckoff position  $q$ , the irreducible representation of which is the element-band representation (EBR), denoted by  $(\rho \uparrow G)_q$ , where  $\rho$  is an irreducible representation of the site-symmetry group,  $G_q$ , of Wyckoff position  $q$ . The irreducible labels of band 7 are  $\Gamma_1-M_1-K_1$  and are consistent with the EBRs  $(E \uparrow G)_{1a}$ , which are obtained by checking the Bilbao Crystallography Server [49]. This proves that band 7 is topologically trivial. The irreducible labels of bands 8 and 9 are  $\Gamma_1 \oplus \Gamma_2-M_1 \oplus M_2-2K_3$ , which can be represented by EBRs  $(A_1 \uparrow G)_{2b}$ . As shown in Fig. 2, the finite lattice structure exposes  $1a$  Wyckoff positions; this is the same as the site-symmetry group of Wyckoff position  $1a$  of band 7. Hence, this will lead to the accumulation of boundary charges, resulting in the appearance of boundary states and corner states in the band gap above and below band 7. That is, we introduce boundary-obstructed topological insulators through the twist angle, which is different from the traditional process of realizing a HOTI [1,2,6–16], which does not require topological phase transitions. The corner states are protected by threefold-rotation symmetry,  $C_3$ . In the same way, the band gaps above and below band 7 in Figs. 1(f) and 1(g) are also OAI.

### III. RESULTS AND DISCUSSION

We next focus on the effect of the twist angle on the boundary and corner states brought about by OAL

bands. First, we perform supercell calculations to determine the projected bands, which consist of 15 unit cells. The resulting projected bands of elastic kagome metamaterials with twist angles of  $35^\circ$ ,  $45^\circ$ , and  $55^\circ$  are shown in Figs. 3(a)–3(c), respectively. A pair of degenerate bands appeared in the band gap in three structures. There will be a pair of degenerate boundary states in the corresponding band gaps above and below band 7 in the metamaterials with twist angles of  $35^\circ$  and  $45^\circ$ . The vibration profiles of these two degeneracy bands are shown in Figs. 3(d) and 3(e), respectively. States with high decay rates are localized on opposite boundaries. The boundary states in the band gap above band 7 have weak locality, which may be due to the narrow band gap, as shown in Fig. 8 (Appendix A). The twist angle has no obvious effect on the boundary states. These phenomena are similar to in-plane degeneracy states achieved by fragile topologies due to Kramers-like degeneracy in self-dual kagome metamaterials, but we confirm that the boundary states and corner states come from the accumulation of fractional charge at the boundary, rather than the fragile topology [43]. When the twist angle increases to  $55^\circ$ , the second degenerate-boundary states disappear due to closing of the band gap.

Then, we further explore the effect of the twist angle on the corner state. We calculate the eigenstates of a finite hexagon-shaped domain, as shown in Figs. 4(b) and 4(c), and its structure and samples are shown in Figs. 1(c)–1(e). Figure 4(a) is the eigenstate of elastic kagome metamaterials with twist angles of  $35^\circ$ . In the band gap, there are four pairs of three degenerate modes on the upper and lower sides of the boundary state. The corresponding vibration modes are shown in Fig. 4(e), and all four types of degenerate modes have localization of deformation at the corners of the hexagon, that is, they form a two-dimensional second-order topological insulator. The corner state comes from charge accumulation at the boundary. Interestingly, the four sets of corner states are localized at different types of corners and have different symmetries. Therefore, according to the position of the corner and the symmetry of the vibration mode, the corner states can be divided into four types, namely, the symmetrical obtuse-corner state, the symmetrical acute-corner state, the asymmetric acute-corner state, and the asymmetric obtuse-corner state. [Notably, the angles of the overall structure are all  $120^\circ$ , and the obtuse angles and acute angles we propose indicate the corresponding inner angles of the lattice, as illustrated in Fig. 2(b)]. However, when the twist angle increases to  $45^\circ$ , there are only two types of corner states, namely, the symmetric obtuse-corner state and the asymmetric obtuse-corner state, as shown in Figs. 4(b) and 4(f). Symmetric acute-corner states and asymmetric acute-corner states are incorporated into boundary states, which can be obtained from the difference (six) in the number of eigenstates corresponding to the boundary states

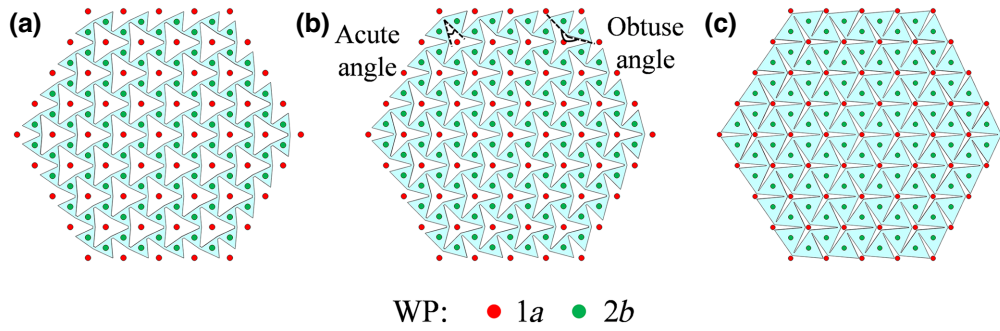


FIG. 2. Wyckoff position on elastic twisted kagome metamaterials with finite lattices of different twist angles: 35° (a), 45° (b), and 55° (c).

in Figs. 4(a) and 4(b). When the twist angle continues to increase to 55°, the asymmetric obtuse-corner state gradually merges into the bulk state, leaving only the symmetric obtuse-corner state, which can be determined by its corresponding vibration mode, as shown in Fig. 4(g). Next, we verified the evolution of the twisted corner versus the corner state, as shown in Fig. 4(d). The six corner states degenerate at the same frequency in the initial kagome lattice ( $\theta = 0$ ). As the twist angle increases, the degenerate corner states split into two types: acute-corner and obtuse-corner states. Upon continuing to increase the twist angle, the asymmetric obtuse-corner states are submerged in edge states.

The previous theoretical discussion has confirmed the emergence of OALs with in-gap corner states in twisted

kagome metamaterials. We then confirmed the theoretical findings discussed above with a series of laser vibrometry experiments performed on a physical prototype. The specific experimental configuration and testing process are shown in Appendix C. The response spectrum of the experimental test is shown in Fig. 5. In a hexagonal domain consisting of kagome lattices with a twist angle of 35°, the existence of four classes of corner states is well-measured experimentally. Due to the highly localized nature of this type of corner state, separate tests for obtuse and acute corners are required. Figure 5(a) shows the response curves of the obtuse corner, from which there are two types of corner states on both sides of the boundary states. Figure 5(b) shows the response spectrum of the acute angle, and there are also corner states on both sides of the boundary state.

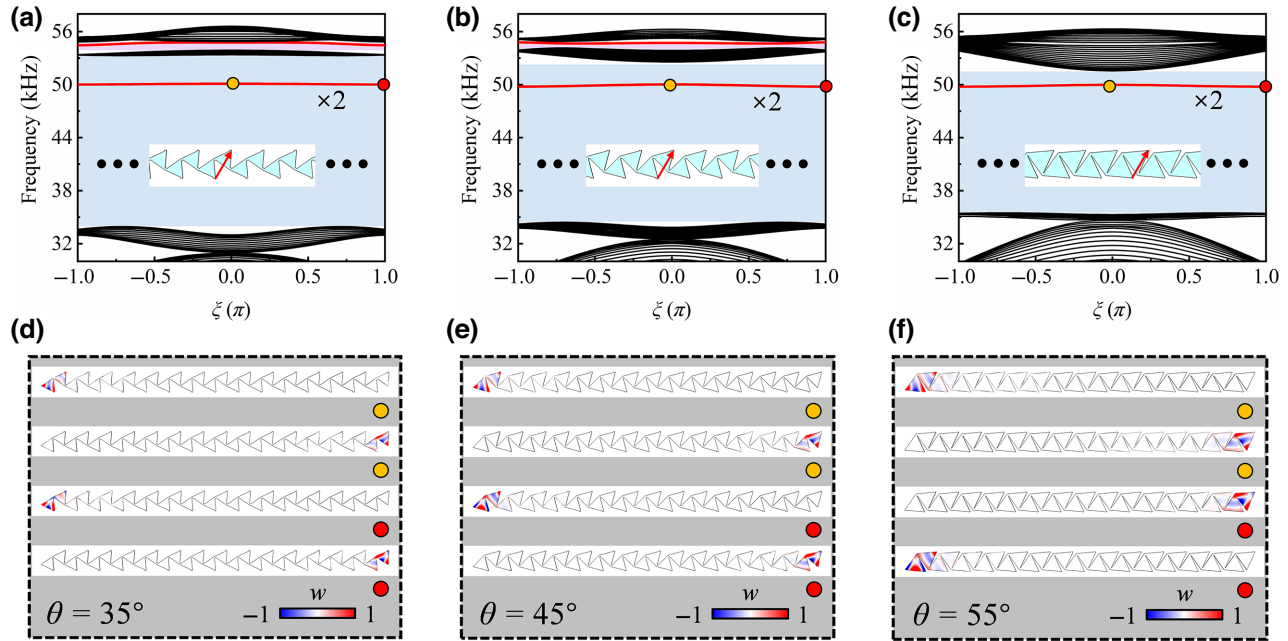


FIG. 3. (a)–(c) Projected band of elastic kagome metamaterials with twist angles of 35°, 45°, and 55°, respectively. (d), (e) Vibration profiles of degenerate edge-state pairs at  $k = 0$  or  $\pi$ , corresponding to the band diagrams in Figs. 2(a)–2(c), which are marked by yellow and red circles, respectively. Color map represents the size of the out-of-plane displacement field ( $w$ ).

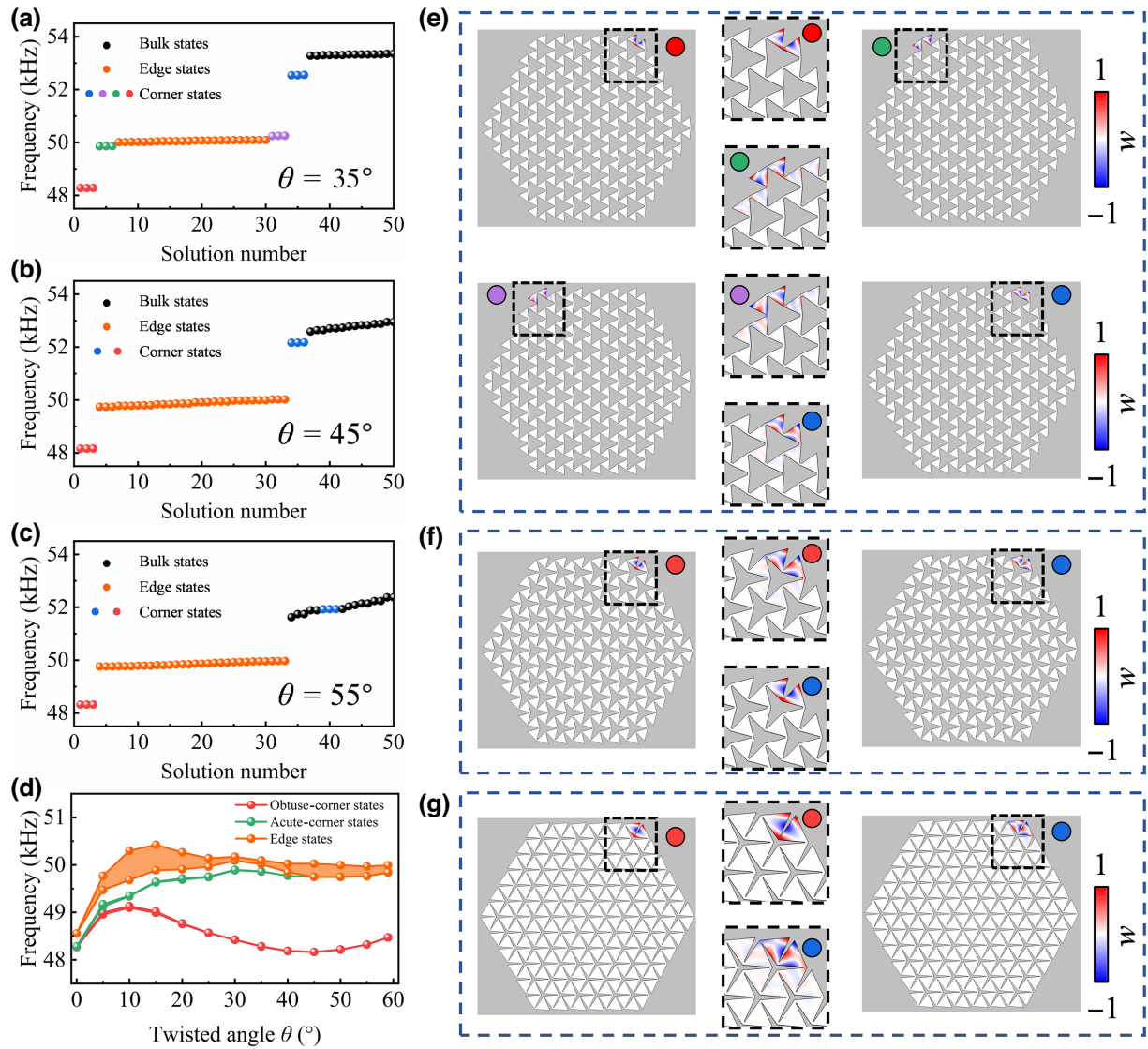


FIG. 4. (a)–(c) Eigenfrequencies of a finite hexagon-shaped domain consisting of elastic kagome metamaterials with twist angles of  $35^\circ$ ,  $45^\circ$ , and  $55^\circ$ , respectively. (d) Effect of twist angle on corner states in elastic kagome metamaterials. (e)–(g) Vibration profiles of corner states for elastic kagome metamaterials with twist angles of  $35^\circ$ ,  $45^\circ$ , and  $55^\circ$ , respectively. Red markers, symmetric obtuse-corner states; green markers, symmetric acute-corner states; purple markers, asymmetric acute-corner states; blue markers, asymmetric obtuse-corner states.

The distribution of the out-of-plane displacement field further confirms the corner states, edge states, and bulk states, as shown in Figs. 5(e)–5(h), 6(a), and 6(b). Experiments will confirm the existence of four classes of corner states. Next, the modulation properties of the twist angle to the corner state are confirmed, and the results are shown in Figs. 5(c) and 5(d). When the twist angle is  $45^\circ$ , only the obtuse-angle state remains, and the acute-corner state is submerged into the edge state; its related response spectrum is shown in Fig. 5(c). Figures 5(i) and 5(j) show the out-of-plane displacement-field distributions of the corresponding obtuse-corner states, which can confirm that the waves can be well localized at the corresponding angles.

The corresponding edge states and bulk states are shown in Figs. 6(c) and 6(d). When the twist angle continues to increase to  $55^\circ$ , only one obtuse-corner state remains, and the other corner state is submerged into the bulk state, as shown in the response spectrum of Fig. 5(d). The out-of-plane displacement-field distributions of the corner states, edge states, and bulk states are shown in Figs. 5(k), 6(e), and 6(f), respectively. In conclusion, the experimental results well validate the theoretical predictions.

#### IV. CONCLUSION

We have confirmed theoretically and experimentally that elastic twisted kagome metamaterials are

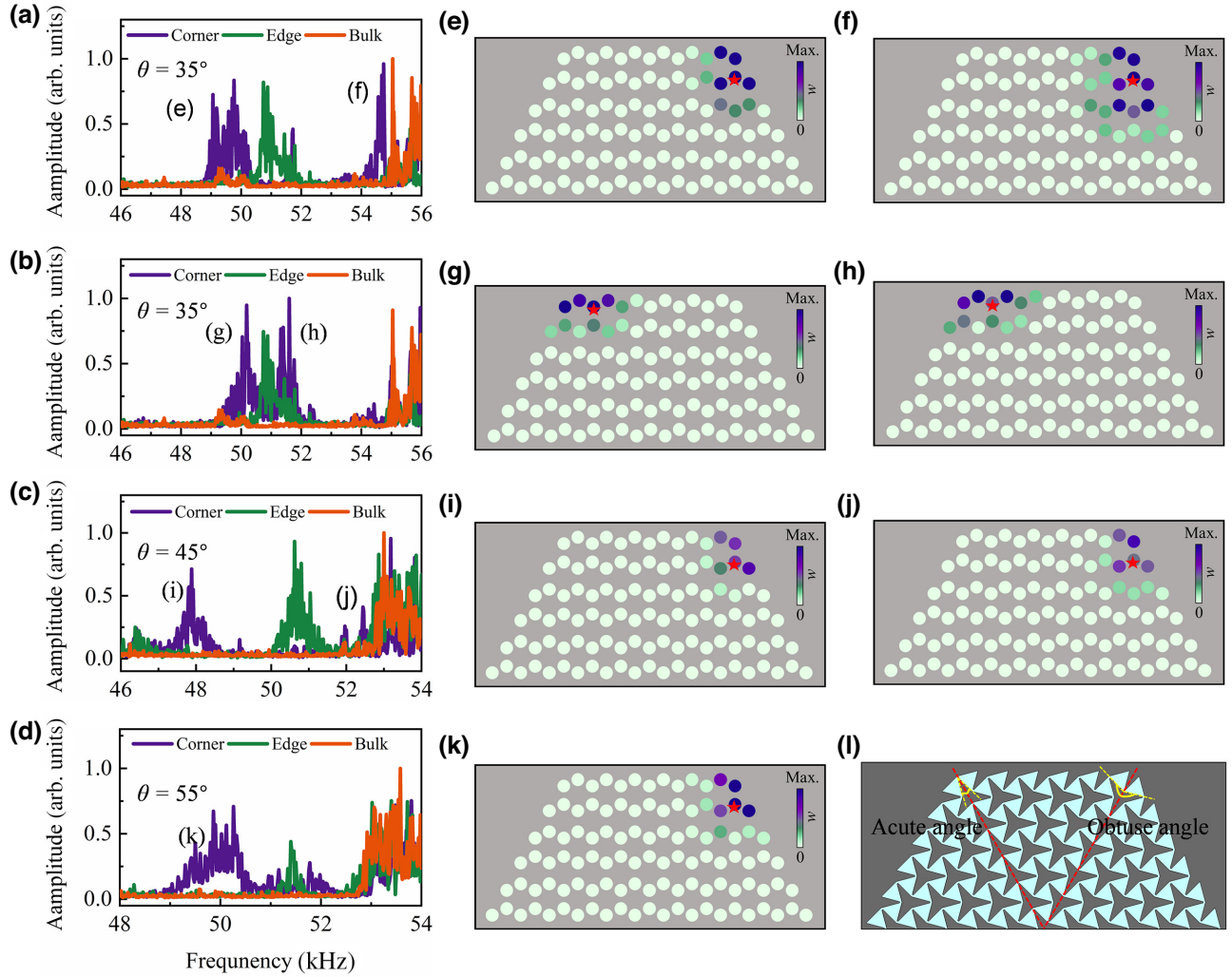


FIG. 5. (a)–(d) Experimentally tested response spectra of the sample at corners, edges, and bulk, where the dark-yellow, green, and purple curves correspond to the response spectra of bulk, edges, and corners, respectively. Experimental samples corresponding to (a)–(d) and the corners tested are as follows: obtuse angle (a) and acute angle (b) of a finite hexagon-shaped domain made from elastic kagome metamaterials with  $35^\circ$  twist angles; obtuse angle of the domain is made from elastic kagome metamaterials with  $45^\circ$  or  $55^\circ$  (c) or  $55^\circ$  (d) twist angles. (e),(f) The  $w$  diagrams of obtuse-corner states of the sample with a twist angle of  $35^\circ$ . (g),(h) The  $w$  diagrams of acute-corner states in the sample with a twist angle of  $35^\circ$ . (i),(j) The  $w$  diagrams of obtuse-corner states in a sample with a twist angle of  $45^\circ$ . (k) The  $w$  diagram of the obtuse-corner state in the sample with a twist angle of  $55^\circ$ . (l) Schematic diagram of the lattice. Red asterisks correspond to the location of the sound source.

boundary-obstructed topological insulators with degenerate boundary states and twist-angle-dependent corner states. We extend the paradigm of studying only in-plane dynamics in thin lattice plates by realizing a second-order topological insulator of flexural waves. The corner states and edge states were confirmed by testing the experimental samples with a laser vibrometer. The twist angle leads to rich and diverse ways to regulate the corner state, where the twist angle can adjust its operating frequency and the frequency difference between the two types of corner states, as well as submerge the corner states in edge states or bulk states. A single OAL band, without being

accompanied by fragile topological bands, will also lead to the emergence of corner states. Hence, we experimentally demonstrate that a fragile topology is not necessary for the emergence of corner states in twisted kagome metamaterials [43,44]. These results show the hidden topological properties in the topologically trivial phase of the boson system and provide an alternative method to realize the boundary-obstructed topological insulator and enrich the control methods and means of obtaining higher-order topological insulators. The twisted kagome lattice is a good reconfigurable platform, which can be used to design reconfigurable corner-state switches [50].

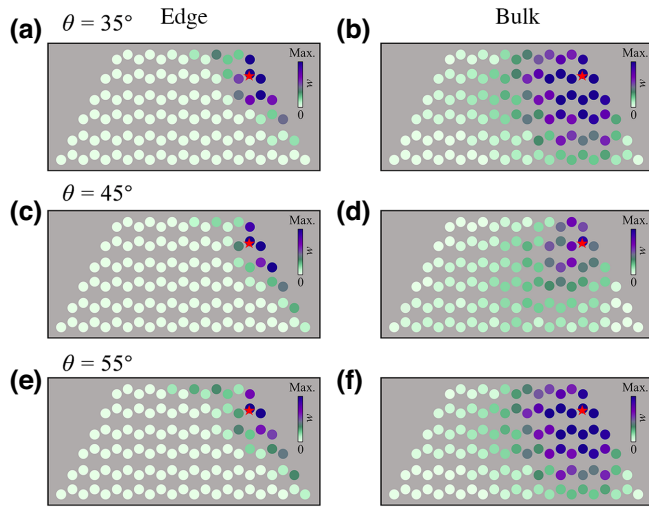


FIG. 6. (a),(c),(e) Out-of-plane displacement-field diagram of edge states obtained from experimental imaging. (b),(d),(f) The  $w$  diagrams of bulk states obtained from experimental imaging. Twist angles corresponding to the samples are as follows: (a),(b)  $35^\circ$ ; (c),(d)  $45^\circ$ ; and (e),(f)  $55^\circ$ .

### ACKNOWLEDGMENTS

The work is jointly supported by the National Key R&D Program of China (Grants No. 2021YFB3801801 and No. 2018YFA0306200) and the National Natural Science Foundation of China (Grants No. 11890702, No. 51721001, and No. 52250363). Z.D.Z. acknowledges support from the China Postdoctoral Science Foundation (Grant No. 2022M711571).

### APPENDIX A: VIBRATION PROFILES OF THE BANDS AT HIGH-SYMMETRY POINTS (HSPs)

Figure 7 displays the vibration profiles of bands 7–9 at the HSPs. The vibration profiles at  $\Gamma$  are odd (even) under horizontal mirror (passing through the center of the unit cell) reflection, corresponding to  $\Gamma_2$  ( $\Gamma_1$ ) representation.  $M$  is only invariant under one of the mirror symmetries that forms the basis of  $M_1$  or  $M_2$  representation, depending on the even or odd symmetry of the modes. The modes at  $K$  are odd (even) under the horizontal mirror, forming  $K_2$  ( $K_1$ ) representation. But the modes at  $K$  transform into each other under mirror reflection and  $C_3$ ; hence, they also form  $K_3$  representation. According to the above symmetry criterion, we confirm the irreducible representation of bands 7–9 at the HSPs, as shown in Fig. 7.

### APPENDIX B: THE DEGENERATE BOUNDARY STATES BETWEEN BAND 7 AND BAND 8

Figure 8 displays the degenerate boundary states corresponding to the band gap between band 7 and band 8. Figures 8(a) and 8(b) show the projected bands of elastic kagome metamaterials with twist angles of  $35^\circ$  and  $45^\circ$ , respectively. Figures 8(c) and 8(d) show vibration profiles of the degenerate boundary state.

### APPENDIX C: EXPERIMENTAL SETUP

The specific test process is as follows. The signal generator sends out a signal amplified by the power amplifier and excites the sound wave through the connected ultrasonic transducer. Then, the laser vibrometer is used to record the vibration signal of the sample, and finally, data acquisition is realized through the acquisition card. In the

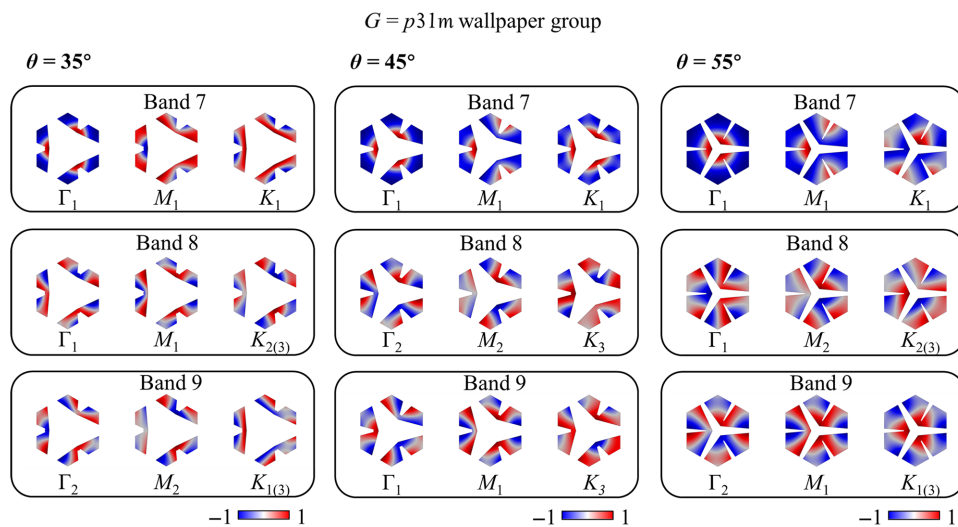


FIG. 7. Vibration profiles of the unit cell corresponding to the eigenfunction at high-symmetry points of  $\Gamma$ ,  $M$ , and  $K$ . Band numbers are counted upwards from the lowest band. Irreducible-representation labels are determined by mode shapes.

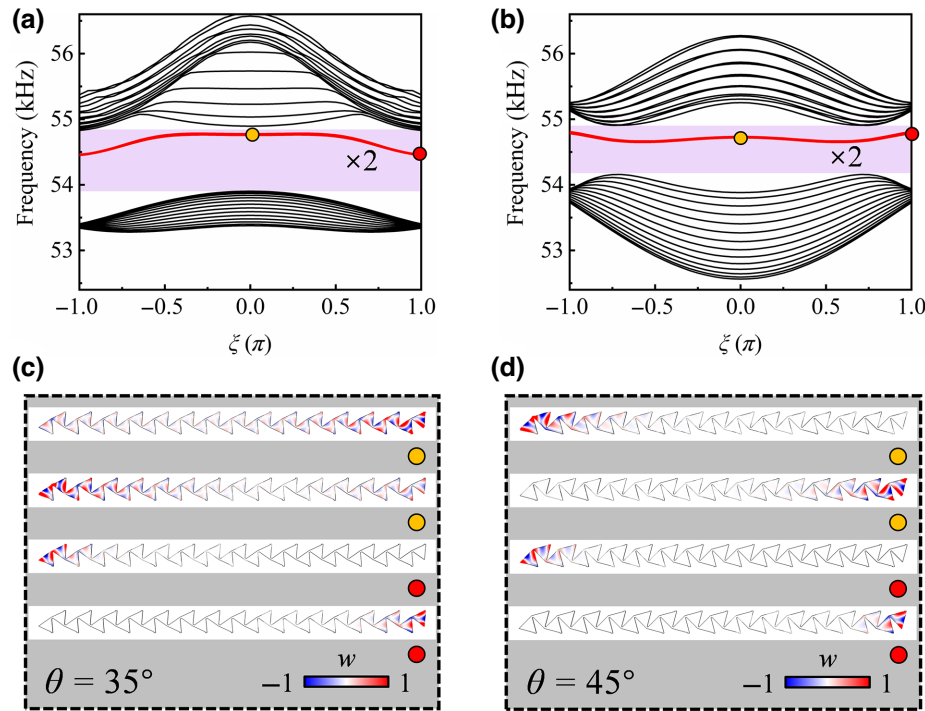


FIG. 8. (a),(b) Projected bands of elastic kagome metamaterials with twist angles of  $35^\circ$  and  $45^\circ$ , respectively. (c),(d) Vibration profiles of degenerate-boundary-state pairs at  $k = 0$  or  $\pi$ , corresponding to band diagrams in (a) and (b), as marked by yellow and red circles, respectively.

experiment, the laser vibrometer is moved by the precise  $X$ - $Y$  two-axis displacement platform to realize the measurement of vibration signals at different positions of the sample, and the whole process is controlled by the LabView program on a computer.

[1] C. W. Peterson, W. A. Benalcazar, T. L. Hughes, and G. Bahl, A quantized microwave quadrupole insulator with topologically protected corner states, *Nature* **555**, 346 (2018).

[2] M. Serra-Garcia, V. Peri, R. Süsstrunk, O. R. Bilal, T. Larsen, L. G. Villanueva, and S. D. Huber, Observation of a phononic quadrupole topological insulator, *Nature* **555**, 342 (2018).

[3] H. Xue, Y. Yang, G. Liu, F. Gao, Y. Chong, and B. Zhang, Realization of an acoustic third-order topological insulator, *Phys. Rev. Lett.* **122**, 244301 (2019).

[4] X. Ni, M. Li, M. Weiner, A. Alù, and A. B. Khanikaev, Demonstration of a quantized acoustic octupole topological insulator, *Nat. Commun.* **11**, 2108 (2020).

[5] X. Zhang, B. Y. Xie, H. F. Wang, X. Xu, Y. Tian, J. H. Jiang, M. H. Lu, and Y. F. Chen, Dimensional hierarchy of higher-order topology in three-dimensional sonic crystals, *Nat. Commun.* **10**, 5331 (2019).

[6] S. Mittal, V. V. Orre, G. Zhu, M. A. Gorlach, A. Poddubny, and M. Hafezi, Photonic quadrupole topological phases, *Nat. Photonics* **13**, 692 (2019).

[7] A. El Hassan, F. K. Kunst, A. Moritz, G. Andler, E. J. Bergholtz, and M. Bourennane, Corner states of light in photonic waveguides, *Nat. Photonics* **13**, 697 (2019).

[8] B.-Y. Xie, G.-X. Su, H.-F. Wang, H. Su, X.-P. Shen, P. Zhan, M.-H. Lu, Z.-L. Wang, and Y.-F. Chen, Visualization of higher-order topological insulating phases in two-dimensional dielectric photonic crystals, *Phys. Rev. Lett.* **122**, 233903 (2019).

[9] X. Zhang, H. X. Wang, Z. K. Lin, Y. Tian, B. Xie, M. H. Lu, Y. F. Chen, and J. H. Jiang, Second-order topology and multidimensional topological transitions in sonic crystals, *Nat. Phys.* **15**, 582 (2019).

[10] X. Ni, M. Weiner, A. Alu, and A. B. Khanikaev, Observation of higher-order topological acoustic states protected by generalized chiral symmetry, *Nat. Mater.* **18**, 113 (2019).

[11] H. Xue, Y. Yang, F. Gao, Y. Chong, and B. Zhang, Acoustic higher-order topological insulator on a kagome lattice, *Nat. Mater.* **18**, 108 (2019).

[12] H. Fan, B. Xia, L. Tong, S. Zheng, and D. Yu, Elastic higher-order topological insulator with topologically protected corner states, *Phys. Rev. Lett.* **122**, 204301 (2019).

[13] Y. Wu, M. Yan, Z. K. Lin, H. X. Wang, F. Li, and J. H. Jiang, On-chip higher-order topological micromechanical metamaterials, *Sci. Bull.* **66**, 1959 (2021).

[14] Y. Qi, C. Qiu, M. Xiao, H. He, M. Ke, and Z. Liu, Acoustic realization of quadrupole topological insulators, *Phys. Rev. Lett.* **124**, 206601 (2020).

[15] M. Serra-Garcia, R. Süsstrunk, and S. D. Huber, Observation of quadrupole transitions and edge mode topology in an  $LC$  circuit network, *Phys. Rev. B* **99**, 020304 (2019).



- [16] S. Imhof, C. Berger, F. Bayer, J. Brehm, L. W. Molenkamp, T. Kiessling, F. Schindler, C. H. Lee, M. Greiter, T. Neupert, and R. Thomale, Topoelectrical-circuit realization of topological corner modes, *Nat. Phys.* **14**, 925 (2018).
- [17] X. Xie, W. Zhang, X. He, S. Wu, J. Dang, K. Peng, F. Song, L. Yang, H. Ni, Z. Niu, C. Wang, K. Jin, X. Zhang, and X. Xu, Cavity quantum electrodynamics with second-order topological corner state, *Laser Photonics Rev.* **14**, 1900425 (2020).
- [18] X. T. He, M. Y. Li, H. Y. Qiu, W. S. Ruan, L. D. Zhou, L. Liu, X. D. Chen, W. J. Chen, F. L. Zhao, and J. W. Dong, In-plane excitation of a topological nanophotonic corner state at telecom wavelengths in a cross-coupled cavity, *Photonics Res.* **9**, 1423 (2021).
- [19] W. Zhang, X. Xie, H. Hao, J. Dang, S. Xiao, S. Shi, H. Ni, Z. Niu, C. Wang, K. Jin, X. Zhang, and X. Xu, Low-threshold topological nanolasers based on the second-order corner state, *Light: Sci. Appl.* **9**, 109 (2020).
- [20] X. Zhang, L. Liu, M. H. Lu, and Y. F. Chen, Valley-selective topological corner states in sonic crystals, *Phys. Rev. Lett.* **126**, 156401 (2021).
- [21] B. Bradlyn, L. Elcoro, J. Cano, M. G. Vergniory, Z. Wang, C. Felsner, M. I. Aroyo, and B. A. Bernevig, Topological quantum chemistry, *Nature* **547**, 298 (2017).
- [22] W. A. Benalcazar, T. Li, and T. L. Hughes, Quantization of fractional corner charge in  $n$ -symmetric higher-order topological crystalline insulators, *Phys. Rev. B* **99**, 245151 (2019).
- [23] T. Li, P. Zhu, W. A. Benalcazar, and T. L. Hughes, Fractional disclination charge in two-dimensional  $C_n$ -symmetric topological crystalline insulators, *Phys. Rev. B* **101**, 115115 (2020).
- [24] S. Vaidya, A. Ghorashi, T. Christensen, M. C. Rechtsman, and W. A. Benalcazar, Topological phases of photonic crystals under crystalline symmetries, *Phys. Rev. B* **108**, 085116 (2023).
- [25] N. Marzari, A. A. Mostofi, J. R. Yates, I. Souza, and D. Vanderbilt, Maximally localized Wannier functions: Theory and applications, *Rev. Mod. Phys.* **84**, 1419 (2012).
- [26] H. C. Po, H. Watanabe, and A. Vishwanath, Fragile topology and Wannier obstructions, *Phys. Rev. Lett.* **121**, 126402 (2018).
- [27] Z. D. Song, L. Elcoro, and B. A. Bernevig, Twisted bulk-boundary correspondence of fragile topology, *Science* **367**, 794 (2020).
- [28] A. Luo, Z. Song, and G. Xu, Fragile topological band in the checkerboard antiferromagnetic monolayer FeSe, *NPJ Comput. Mater.* **8**, 26 (2022).
- [29] G. F. Lange, A. Bouhon, and R. J. Slager, Subdimensional topologies, indicators, and higher order boundary effects, *Phys. Rev. B* **103**, 195145 (2021).
- [30] J. Herzog-Arbeitman, Z. D. Song, N. Regnault, and B. A. Bernevig, Hofstadter topology: Noncrystalline topological materials at high flux, *Phys. Rev. Lett.* **125**, 236804 (2020).
- [31] L. Wang, Y. Jiang, J. Liu, S. Zhang, J. Li, P. Liu, Y. Sun, H. Weng, and X. Q. Chen, Two-dimensional obstructed atomic insulators with fractional corner charge in the  $MA_2Z_4$  family, *Phys. Rev. B* **106**, 155144 (2022).
- [32] D. S. Ma, K. Yu, X. P. Li, X. Zhou, and R. Wang, Obstructed atomic insulators with robust corner modes, *Phys. Rev. B* **108**, L100101 (2023).
- [33] X. Mao and T. C. Lubensky, Maxwell lattices and topological mechanics, *Annu. Rev. Condens. Matter Phys.* **9**, 413 (2018).
- [34] C. L. Kane and T. C. Lubensky, Topological boundary modes in isostatic lattices, *Nat. Phys.* **10**, 39 (2014).
- [35] D. Rocklin, S. Zhou, K. Sun, and X. Mao, Transformable topological mechanical metamaterials, *Nat. Commun.* **8**, 14201 (2017).
- [36] H. Chen, H. Nassar, and G. L. Huang, A study of topological effects in 1D and 2D mechanical lattices, *J. Mech. Phys. Solids* **117**, 22 (2018).
- [37] Y. Chen, X. Liu, and G. Hu, Topological phase transition in mechanical honeycomb lattice, *J. Mech. Phys. Solids* **122**, 54 (2019).
- [38] K. Sun and X. Mao, Continuum theory for topological edge soft modes, *Phys. Rev. Lett.* **124**, 207601 (2020).
- [39] M. Fruchart, Y. Zhou, and V. Vitelli, Dualities and non-Abelian mechanics, *Nature* **577**, 636 (2020).
- [40] H. Danawe, H. Li, K. Sun, and S. Tol, Finite-frequency topological Maxwell modes in mechanical self-dual kagome lattices, *Phys. Rev. Lett.* **129**, 204302 (2022).
- [41] H. Danawe, H. Li, H. Al Ba'ba'a, and S. Tol, Existence of corner modes in elastic twisted kagome lattices, *Phys. Rev. B* **104**, L241107 (2021).
- [42] P. Azizi, S. Sarkar, K. Sun, and S. Gonella, Dynamics of self-dual kagome metamaterials and the emergence of fragile topology, *Phys. Rev. Lett.* **130**, 156101 (2023).
- [43] Y. F. Chen and D. X. Yao, Fragile topological phase on the triangular kagome lattice and its bulk-boundary correspondence, *Phys. Rev. B* **107**, 155129 (2023).
- [44] Q. L. Lei, W. Zheng, F. Tang, X. Wan, R. Ni, and Y. Q. Ma, Self-assembly of isostatic self-dual colloidal crystals, *Phys. Rev. Lett.* **127**, 018001 (2021).
- [45] Q. L. Lei, F. Tang, J. D. Hu, Y. Q. Ma, and R. Ni, Duality, Duality, hidden symmetry and dynamic isomerism in 2D hinge structures, *Phys. Rev. Lett.* **129**, 125501 (2022).
- [46] S. Gonella, Symmetry of the phononic landscape of twisted kagome lattices across the duality boundary, *Phys. Rev. B* **102**, 140301 (2020).
- [47] M. Charara, K. Sun, X. Mao, and S. Gonella, Topological flexural modes in polarized bilayer lattices, *Phys. Rev. Appl.* **16**, 064011 (2021).
- [48] Bilbao Crystallogr. Server, "Bandrep: Band representations of the double space groups," (2017). <https://www.cryst.ehu.es/cgi-bin/cryst/programs/bandrep.pl>.
- [49] M. Schaeffer and M. Ruzzene, Wave propagation in reconfigurable magneto-elastic kagome lattice structures, *J. Appl. Phys.* **117**, 194903 (2015).
- [50] M. Ezawa, Higher-order topological insulators, and semimetals on the breathing kagome and pyrochlore lattices, *Phys. Rev. Lett.* **120**, 026801 (2018).